Conformational and Packing Modeling of Optically Active Polyesters. 2. Helical Structure of an Isotactic Polylactone

Ziru He and Robert E. Prud'homme*

Département de chimie, Centre de recherche en sciences et ingénierie des macromolécules, Université Laval, Sainte-Foy, Québec, Canada G1K 7P4

Received October 1, 1998; Revised Manuscript Received July 26, 1999

ABSTRACT: Optically active poly(α-methyl-α-*n*-propyl-*β*-propiolactone) (PMPPL) crystallizes in a 2_1 helical conformation, but its conformational structure and packing symmetry have not been solved and refined yet. On the basis of the rotational isomeric state approximation and the conformational algorithm for polymer helices, optimum conformational models derived from single helices were used as a starting point in building crystal structures. Both intra- and intermolecular interactions were simultaneously optimized. Semiempirical molecular mechanics calculations of an isotactic single chain having fixed experimental helical parameters revealed that the preferred conformation for PMPPL entails the ttg^-g^- backbone chain conformation with a g–t side-chain orientation. Crystal models compatible with the observed orthorhombic lattice dimensions ($a = 10.6$, $b = 11.1$ Å) were built and refined against electron diffraction data, X-ray powder diffraction spectra, and structure factor calculations. The favored structure contains two 2-fold screw helices packed antiparallel in an orthorhombic lattice with space group $P2_12_12_1-D_2^4$. With the ttg^-g^- main chain conformation, both the g–t and tt conformations are possible for the side chain according to the refinement of X-ray structure factors. However, the g–t side-chain conformation shows a better fit than that of the tt conformation with the electron diffraction patterns. The flexible procedure of energy minimization yields distinct values of fiber period for the g–t and tt conformations, e.g., 6.31 and 6.14 Å, respectively. The final discrepancy *R* factors are 0.20 for the g–t and 0.17 for the tt side-chain models when compared to X-ray data and 0.17 for the g–t and 0.27 for the tt side-chain models when compared to electron diffraction data.

Introduction

Polyesters[1−7] comprising an asymmetric carbon atom in their backbone exhibit optically active properties and often lead to the formation of stereocomplexes. These polymers show interesting conformational changes and polymorphism. Poly(α-methyl-α-*n*-propyl-*β*-propiolactone) (PMPPL) and poly(α-methyl-α-ethyl-*β*-propiolactone) (PMEPL)[1−4] are representative examples of this family and show similarities in structure and behavior with polylactides.[5−7]

Isotactic PMPPL and PMEPL exhibit planar zigzag (all-trans) or helical conformations depending on their preparation methods. Electron diffraction[1] and X-ray powder diffraction[3] patterns have led to cell parameters, but the limited number of reflections in both cases did not allow an accurate solution. Structurally, there are 21 atoms in each repeat unit of PMPPL, and even if the constrained least-squares method[9,10] is used to refine the crystal structure, the number of adjustable parameters is too large as compared to the limited number of observed independent reflections. Moreover, the packing symmetry has not been defined yet. Without additional information from packing analysis and energy calculation, it is difficult to define a reliable conformational structure and packing symmetry from experiments.

As a first step in our efforts at modeling poly(*β*-propiolactones) derivatives, the planar zigzag structure of PMEPL has been resolved and refined in a previous paper[8] with conformational modeling methods. In the literature, both the two-[8,11] and single-step procedures[8,12−15] have led to similarly acceptable results starting from the extended backbone conformation known from experiments. It is the purpose of this paper to similarly solve and refine the helical structure of PMPPL, which is preferred here to PMEPL because of the better quality of the electron diffraction data available.

However, the question arises whether the two- or single-step procedure is more appropriate in this case. In principle, the single-step method is straightforward if the helical symmetry condition (here, the helical advanced distance and 2_1 helix) can be fixed during the energy minimization. In practice, however, it is difficult to implement because (1) there is no such commercial software package currently available and (2) it requires the elimination of many conformations, which is very time-consuming. On the other hand, the two-step procedure, in combination with crystallographic data, is a fast method that permits the exclusion of unreasonable conformations, but it separates intra- and intermolecular interactions and, thus, yields usually less accurate final results for polymer helical structures.

The choice of a fast and simple algorithm for computer modeling is also problematic. Even for polylactides,[5,6] which have a shorter repeat unit than poly(*β*-propiolactones), the three-dimensional conformational space had to be energetically scanned before proposing four possible starting conformations for the 3_1 helix.[5] The situation is more complicated in the case of PMPPL. Four dihedral angles along the backbone and two dihedral angles along the side chain increase considerably the number of degrees of freedom as compared to the case of polylactides.

Fortunately, for most linear polymers, the fiber period is readily determined by electron and X-ray diffraction measurements, and if all the chemical units are assumed to be equivalent in the crystal, reasonable

* To whom correspondence should be addressed.

10.1021/ma981549+ CCC: $18.00 © 1999 American Chemical Society
Published on Web 10/09/1999

structure models can be selected. Therefore, the conformational helical algorithm[16,17] can be used for finding optimum starting conformations that satisfy the measured helical parameters. By use of this algorithm, two backbone dihedral angles can be calculated exactly, but the other two dihedral angles have to be determined by a conformational grid search, to find the most probably discrete conformations.[18,19]

In this paper, a helical single PMPPL chain is built and energetically evaluated. Local-energy minimum conformations of reasonable geometry are considered as starting points in building crystal lattices. The two- and single-step procedures are both used together. The former is used to eliminate unreasonable starting conformations and packing forms based on energy minimization and electron diffraction simulations. Final structures are obtained using the second approach and refined against electron diffraction data, X-ray powder diffraction spectra, and structure factor calculations.

Method of Calculation

Single helical chains were energetically evaluated following the procedure previously developed.[8] However, in our previous work, the backbone conformation was fixed in the trans state on the basis of experimental results, whereas in the present study, the backbone conformation was not known, except that it is a 2_1 helix with a specific helical distance. For practical reasons, an approximate, stepwise procedure was adopted in place of the more rigorous approach.[13−15]

All calculations and simulations were based on the polymer consistent force field (PCFF)[20] and the Insight II and Discover simulation softwares (MSI) and were carried out on a Silicon Graphics INDIGO II workstation. A cutoff limit of 12 Å was applied for the nonbonded interactions of both the isolated chain and crystalline structure. The dipole moments of the ester, methyl, and methylene groups were decomposed into atomic partial charges, and the net atomic charge of each repeat unit was 0. The energy terms were calculated and the minimizing procedure was carried out as in the previous paper.[8]

Isolated Chain. To solve the crystal structure, the backbone conformation, side-chain conformation and packing symmetry of the crystal need to be defined. Conformational grid search is a classical method of generating minimum-energy conformations for an isolated single chain. This step is helpful because it allows for the exclusion of unreasonable conformations. With the retained conformations, average internal coordinates can be obtained and used in the conformational algorithm[16,17] for polymer helices, because it is necessary to perform a more systematic conformational grid search at the fixed helical symmetry conditions.

The stepwise procedure started by finding preferential minimum-energy conformations for the backbone chain using the conformational grid search. Solid-state ^{13}C nuclear magnetic resonance spectroscopy[1,3] revealed that PMPPL exists as a 2_1 helix and three repeat units were used as a fragment of the single chain. In Figure 1a is shown the repeat unit used in the calculation with atomic numeration, whereas Figure 1b illustrates the corresponding model compound with three repeat units. There are four dihedral angles (τ, ψ, η, and Φ) along a backbone chain for each repeat unit. The corresponding Fischer projection with two repeat units is also given on the right-hand side of the figure.

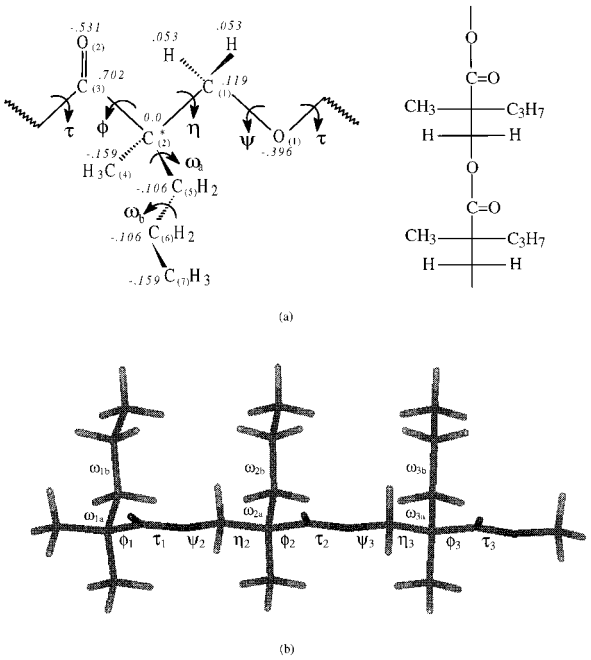

Figure 1. Model structures with their dihedral angles: (a) conformational repeat unit with *R* chirality, atomic partial charges, and Fischer projection and (b) model compound used for conformational analysis.

In crystals, each asymmetric repeat unit was assumed to have the same atomic environment, and therefore, $\omega_{1a} = \omega_{2a} = \omega_{3a}$, $\omega_{1b} = \omega_{2b} = \omega_{3b}$, $\tau_1 = \tau_2 = \tau_3$, $\psi_2 = \psi_3$, $\eta_2 = \eta_3$, and $\Phi_1 = \Phi_2 = \Phi_3$, as done for the crystal structures of optically active polyamides.[21] Moreover, for the partial double bond (C═O)−O, because the planar trans conformation is strongly preferred to the planar cis conformation,[18,19] it was reasonable to assume $\tau_1 = \tau_2 = \tau_3 = 180°$ in a coarser grained approach. Three discrete isomeric states[18,19] (trans, gauche 60°, and gauche −60°) were initially considered for the torsion of the side chain. Therefore, $\omega_a\omega_b$ could have nine conformations: tt, tg, tg–; gt, gg, gg–; and g–t, g–g, g–g–. A full-relaxation optimization[12−15,8] was then used to calculate potential energy surfaces of the model compound for the nine side-chain models. Torsion angles ψ, η, and Φ were varied using a grid of 30° from −180 to 180°. For clarity, the superscript (−) is hereafter used to refer to the main chain and the subscript (−) is used to refer to the side chain.

(a) Determination of Torsion Angles for the Side Chain. The coarse conformational grid search mentioned above for the backbone of the model compound produced more than 200 local energy minima for the nine side-chain models. However, only ttgg (in the following order: τ, ψ, η, and Φ) and ttg$^-$g$^-$ backbone conformations with the g–t, gt, and tt side chains are both energetically preferred and geometrically suited to a 2_1 helix having the observed fiber period of 6.7 Å[1] (although it is clear that this value is overestimated[22,23]). These two backbone conformations were, therefore, considered as starting points for a more precise determination of side-chain orientations, and a grid search was performed varying ω_a and ω_b at 10° intervals, between −180 and 180°.

Energy minimization yielded two energy contour maps for the ttgg and ttg$^-$g$^-$ backbones as a function of torsion angles ω_a and ω_b, which were calculated using the Boltzmann factor:

$$\omega = \frac{\sum_{i=1}^{n}\sum_{j=1}^{3}\omega_{ij}e^{-(E_{ij}-E_o)/RT}}{\sum_{i=1}^{n}\sum_{j=1}^{3}e^{-(E_{ij}-E_o)/RT}} \quad (1)$$

where E_o corresponds to the lowest energy among all energy minima of the two contour maps and E_{ij} denotes the potential energy of a local energy minimum of dihedral angle ω_{ij} for a specified backbone conformational state i (e.g., ttg$^-$g$^-$) with a side-chain conformational state j (e.g., g$_-$t). The summation was performed for n backbone samples, and three discrete states were considered for each torsion. The calculated ω_a and ω_b values were used for the final energy evaluation of a single chain.

(b) Determination of Backbone Torsion Angles Using the Conformational Helical Algorithm.[16,17] The attempts of energy optimization mentioned above fulfilled two purposes: one is that the torsion angles of the side chain have been approximately determined as discrete values; the other is that statistically averaged backbone internal coordinates (bond lengths and angles) have been determined from local minimum-energy conformations. The averaged bond lengths produced from this conformational grid search are 1.54, 1.56, 1.42, and 1.36 Å for C(3)−C(2), C(2)−C(1), C(1)−O(1), and O(1)−C(3), respectively; the averaged bond angles are 110.6, 106.5, 109.3, and 119.3° for O(1)−C(3)−C(2), C(3)−C(2)−C(1), C(2)−C(1)−O(1), and C(1)−O(1)−C(3), respectively.

A coarse conformational grid search for the backbone is, of course, insufficient to produce accurate 2_1 helical conformations having the fiber period of 6.7 Å. Moreover, the partial double bond (C═O)−O has been confirmed to show deviations of several degrees from the standard planar trans conformation.[12] A more precise grid search at 5° intervals was then applied to the backbone torsion angles τ (180 ± 10°) and Φ (−180 ∼ 180°). The two other torsion angles ψ and η could be exactly calculated using the conformational helical equations[16,17] for polymer helices according to the measured helical parameters. Series of four torsion angles were produced by the developed C-program and introduced into Discover by modifying the input files using Tcl scripts.

Crystal Model Building and Refinement. Different packing forms in the $P2_12_12$ and $P2_12_12_1$ space groups were examined by both energy analysis and diffraction simulations. Energy computations were performed using the same parameters as those for the single chain. In a first step, the initial geometry (bond lengths, bond angles, and torsion angles) and unit cell parameters were kept fixed during the search of the space group and starting conformations. The relative position of the chain along the fiber axis and its setting angle were varied until reaching the lowest energy and reasonable electron diffraction patterns. The final crystal structure was established by simultaneously minimizing both intra- and intermolecular interactions and was refined against electron diffraction data, X-ray powder diffraction spectra, and structure factor calculations. The calculations of structure factors and discrepancy factor R were made as was done in previous reports.[8,10] The overall isotropic thermal factor B was chosen from 0 to 30 Å^2, depending if R had reached its lowest value.

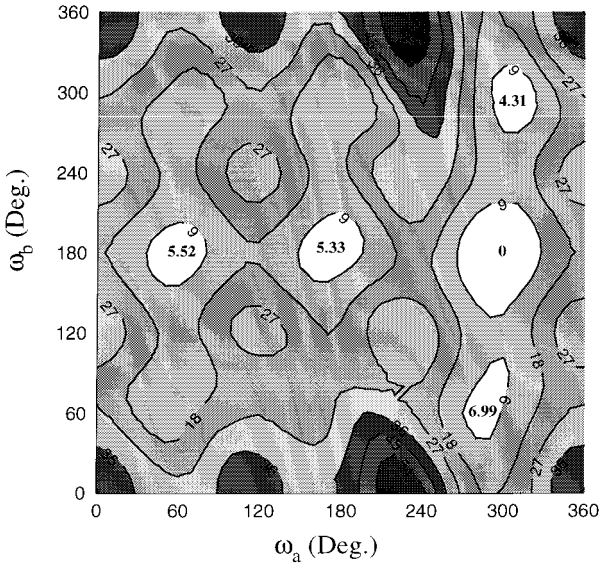

Figure 2. Potential energy contour map of the 2_1 helical ttg$^-$g$^-$ backbone conformation as a function of the side-chain rotation angles. All data are given relative to the lowest energy (48.89 kcal/mol) g$_-$t side-chain conformation. In this map, energy increases when going from a light to a darker color.

From the electron diffraction patterns reported previously,[1] the intensities were digitized from the original negatives with SigmaScan image analysis version 2.0 software (Jandel Scientific) and a microscope, and the background around each spot was removed. Neither polarization corrections (unknown in electron diffraction) nor Lorentz corrections have been performed in this study, although quasi-Lorentz corrections could account for the effect of crystal geometry in diffraction intensity measurements.[24]

Results and Discussion

Conformational Energy Calculations. The coarse conformational grid search for the three backbone torsion angles (ψ, η, and Φ) resulted in two most probable 2_1 backbone conformations, ttg$^-$g$^-$ and ttgg ($\tau = \psi = 180°$, $\eta = \Phi = \pm 60°$), for the nine side-chain models. It should be noted that ttgg and ttg$^-$g$^-$ are distinct helical forms because there is a chiral carbon atom in the isotactic main chain. These two backbone conformations have the same fiber period (6.7 Å) as the earlier experiment.[1] Among the nine possible side-chain conformations, the g$_-$t, gt, and tt are by far energetically preferred to the others. The ttg$^-$g$^-$/g_t (i.e., backbone/side-chain) conformation is that of lowest energy, while other favored 2_1 conformations are: ttgg/g_t with 3.56, ttg$^-$g$^-$/gt with 5.52, ttgg/gt with 4.14, ttg$^-$g$^-$/tt with 5.79 and ttgg/tt with 4.98 kcal/mol. All data are reported relative to the 48.89 kcal/mol value of the ttg$^-$g$^-$/g_t conformation. For each side-chain model, the all-trans backbone chain has a higher energy than the corresponding ttgg and ttg$^-$g$^-$ conformations, except for the tt side chain where the energy difference is 2.83 kcal/mol (tttt/tt).

The grid search for the side-chain torsion angles also revealed that g$_-$t is the most probable side-chain conformation and ttg$^-$g$^-$ is the most energetically preferred backbone conformation. Three discrete isomeric states were clearly identified for both ω_a and ω_b in each of the two energy contour maps (for ttgg and ttg$^-$g$^-$). Figure 2 illustrates the potential energy contour

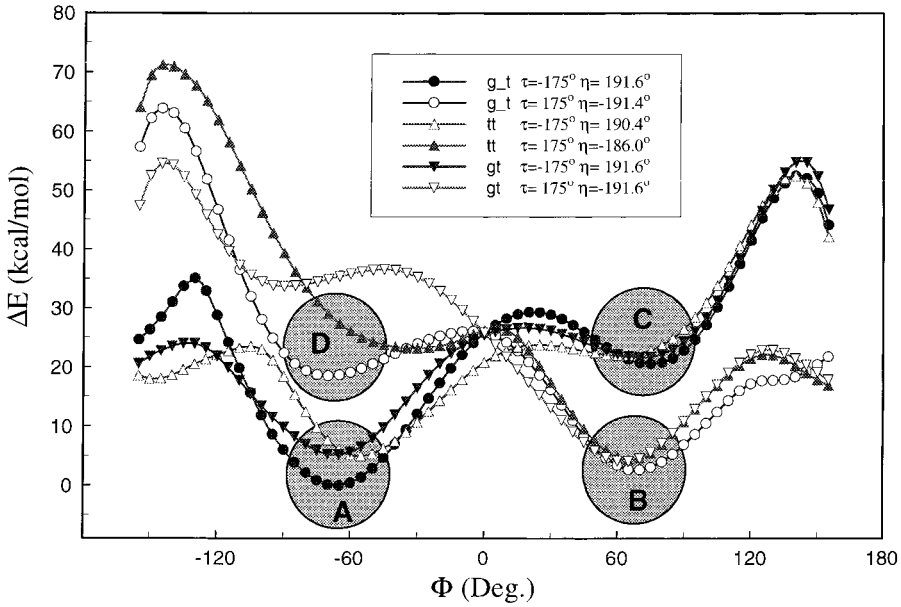

Figure 3. Potential energy curves as a function of angle ϕ for the g–t, tt, and gt side chains. Only two backbone helical directions (ttg–g– and ttgg) with the lowest energy minimum for τ are illustrated. Each point corresponds to a 2-fold screw backbone conformation. Corresponding backbone torsion angles for the minimum-energy conformations are listed in Table 1 for the backbone conformations ttg–g– and ttgg.

map for the ttg$^-$g$^-$ backbone conformation. By eq 1, values of side-chain rotation angles were calculated and found to be very close to the values of +180°, +60°, and −60° assumed in the coarse scan.

By use of the calculated averaged bond lengths and averaged bond angles for the backbone, the conformational helical algorithm was used to find more precise backbone torsion angles. Because the torsion angles τ and Φ were assumed to have specific values, ψ and η could be calculated quantitatively. Therefore, the grid search for τ and Φ produced a series of corresponding ψ and η values; thousands of backbone torsion angles produced from the helical algorithm were introduced into Discover and evaluated energetically for the nine side-chain models. For each side-chain model, only a minor deviation (±10°) from 180° was investigated for τ (there are two different helical directions because of the existence of a chiral center). With the g_t, tt, and gt side chains as examples, potential energy curves are illustrated in Figure 3 as a function of Φ. Each point refers to a 2-fold screw conformation having a measured fiber period of 6.7 Å.

From the calculations, it was found that each side chain exhibits two distinct curves of lowest energy corresponding to negative and positive deviations of the τ angle; from Figure 3, it was found that each of those curves exhibits two energy minima related to different backbone conformations. The four backbone conformations with the local energy minima depicted in Figure 3 are described as model A for ttg$^-$g$^-$, model B for ttgg, model C for tgtg, and model D for tg$^-$tg$^-$.

Figure 4 depicts the geometrical difference between the four backbone models with a g–t side chain. It is seen that two carbonyl bonds in each helical period in models A and B are nearly antiparallel. This arrangement considerably reduces the intramolecular electrostatic energy as compared to the C and D models where the two carbonyl bonds are far from the antiparallel arrangement, with the intramolecular energies being thus increased to above 20 kcal/mol.

There is a total of 36 minima for the nine side-chain models. However, the backbone models C and D were immediately eliminated due to energies at least 20 kcal/mol higher than the lowest energy minimum. Other eliminated side-chain models are tg, gg, tg–, and gg– due to the higher energies (at least 10 kcal/mol). Table 1 gives the torsion angles and relative energies for the other 10 conformations. All models referred to hereafter are named using the side-chain conformation as a prefix and the backbone conformation as a suffix. For example, g–tA indicates a g–t side-chain and a ttg$^-$g$^-$ backbone conformation (model A). It should be noted, from Table 1, that in all cases Φ deviates from 180° by more than 20°; otherwise it is impossible to reach a 2_1 helix with a fiber period of 6.7 Å when τ is constrained within 180 ± 10°.

Several conclusions can be drawn from Figure 3 and Table 1: (1) The g–tA conformation is the preferred model, and its energy (49.85 kcal/mol) is very close to that of the lowest minima found in the grid search (48.89 kcal/mol). The minor difference stems from the use of slightly different values of the four backbone torsion angles and averaged internal coordinates instead of optimized internal coordinates under the force field for the g–tA conformation. Theoretically, this small but significant inconsistency of about 1 kcal/mol could be avoided if a rigorous procedure could be used. (2) For the partial double bond C(=O)−O, the torsion angle τ deviates from 180°, typically by about 5°, which is comparable with the findings of an earlier study.[21] (3) The second side-chain torsion angle ω_2 preferentially adopts a trans rather than a gauche conformation, because the latter gives an interference between the backbone and side chains. (4) The ttg$^-$g$^-$ and ttgg conformation are by far energetically preferred to the tgtg and tg$^-$tg$^-$. Geometrically, all of the 36 models can be considered as starting conformations; however, only those models given in Table 1, corresponding to lower energies, were examined as trial structures for packing.

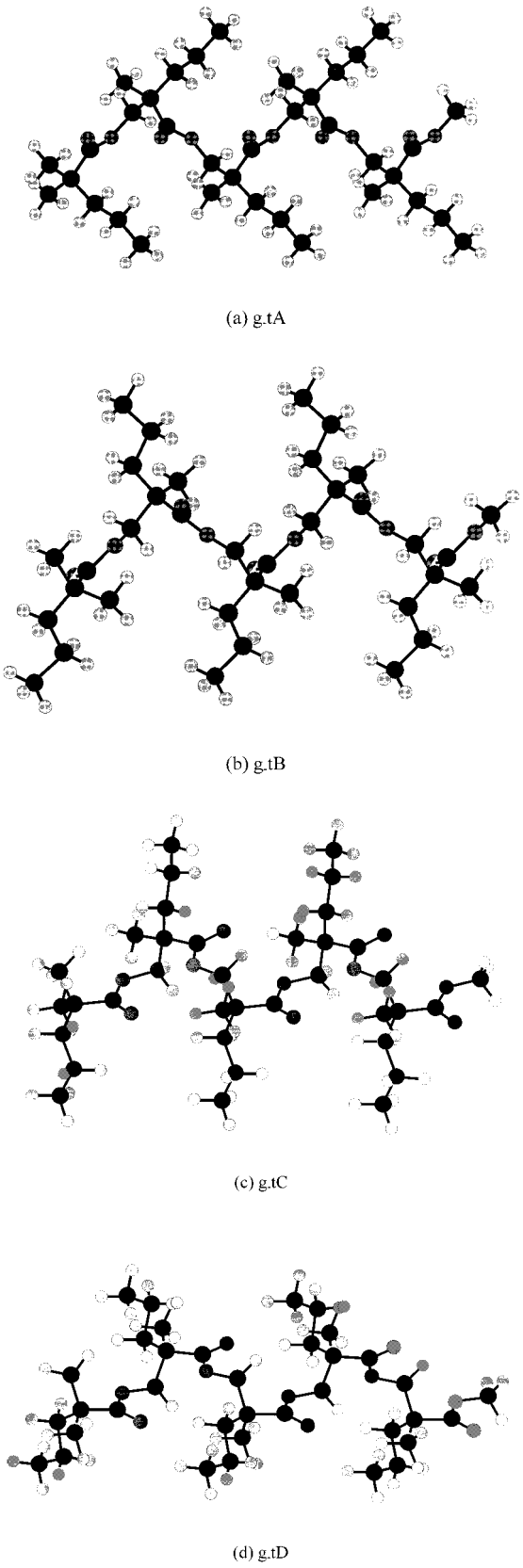

Figure 4. Four local minimum-energy conformations with the observed 2_1 helical parameters (6.7 Å) for the g–t side chain: (a) g–tA, (b) g–tB, (c) g–tC, and (d) g–tD.

Chain Packing for Different Models. In the electron diffraction patterns,[1] the principal reflections (110, 210, 200, and *h*21) were observed, and they were indexed by an orthorhombic unit cell having dimensions $a = 10.6$, $b = 11.1$, and $c = 6.7$ Å (fiber period). The weak 320 reflection and the *h*42 layer line could be observed in the original negative films. If four repeat units are assumed in the unit cell, the calculated density is 1.08 g/cm^3, which is close to the observed value of 1.10 g/cm^3. The systematic absences are *h*00 when *h* is odd and 0*k*0 when *k* is odd, but 00*l* reflections cannot be ascertained. From these data, the most acceptable space group is $P2_12_12_1-D_2^4$ or $P2_12_12-D_2^3$ (see Table 4.1.9 of International Tables of X-ray Crystallography[25]), which both lead to an antiparallel packing of the chains. The molecular chain contains two repeat units per identity period, and two molecular chains pass through the unit cell. Both space groups have four equivalent general positions because the chain axis must coincide with a 2-fold screw axis of the space group.

However, $P2_12_12-D_2^3$ can easily be excluded from the simulation, because $P2_122_1$ and $P22_12_1$ resulted in incompatible results with experimental data for any kind of side-chain or backbone models: strong 110 and 210 reflections are missing in the simulated patterns. On the other hand, each chain contains chiral centers along the backbone and the chain has direction; thus, $P2_12_12$ is also an unacceptable space group due to the incompatibility between the 2_1 helix and the 2-fold axis. Moreover, the presence of *hk*0 reflections ($h + k = 2n$) is incompatible with the experimental results (i.e., with the presence of 210). Therefore, the symmetry of the space group should arise from $P2_12_12$ to $P2_12_12_1$. In fact, if $P2_12_12_1$ is a reasonable space group, $P2_12_12$ could be excluded on the basis of its lower symmetry.

After energy minimization of different rigid packing models, the *hk*0 electron diffraction patterns were simulated for the most stable packing structures. The most intense reflections are reported in Table 2. It is found that the g–tA and gtB models result in patterns in good agreement with the observations. The structural difference between these two models can be seen in Figure 5, where the carbonyl bond is adjacent to the propyl side chain in the g–tA model, whereas this bond is very close to the methyl group (instead of the propyl group) in the gtB model. The same relation was found between the ttA and ttB models (Figure 5). However, the ttA model has a weaker 200 reflection than that observed in ttB, and the ttB model has a stronger 320 reflection than that in ttA and an additional intense 120 spot. Nevertheless, the ttA and ttB models were kept as trial structures for the flexible energy minimization, because the cooperativity between intra- and intermolecular interactions may change intensities in some way. Other models shown in Table 2 were eliminated due to considerable deviation from the observed *hk*0 patterns and higher packing energies when compared to the intramolecular energies of the single chain.

The flexible energy optimization and diffraction simulation performed for the g–tA, gtB, ttA, and ttB models allowed for the elimination of two models: gtB and ttB. For the gtB model, the strong 210 reflection disappears and the projection of the two chains along the *c* axis becomes parallel, whereas for the ttB model, the 320 reflection is still strong. Moreover, 120 and 042 reflections are much stronger than observed. The g–tA and ttA models led to more acceptable results with the electron diffraction as well as with X-ray data.

Refinement of the g–tA and ttA Models. The previous trial-and-error procedure led us to retain the $P2_12_12_1$ space group, the ttg–g– backbone conformation,

Table 1. Torsion Angles of the PMPPL Chain Backbone Corresponding to the 10 Lower Minimum-Energy Conformations[a]

	side chain									
	g–t		tt		gt		g–g		g–g–	
model	g–tA	g–tB	ttA	ttB	gtA	gtB	g–gA	g–gB	g–g–A	g–g–B
τ (°)	−175.0	175.0	−175.0	170.0	−175.0	175.0	−175.0	175.0	−175.0	175.0
ψ (°)	191.6	−191.4	190.4	−186.0	191.6	−191.6	191.4	−191.4	191.6	−190.6
η (°)	−58.5	53.6	−68.1	58.3	−58.5	58.5	−53.6	53.6	−58.5	48.8
ϕ (°)	−65.0	70.	−55.0	65.0	−65.0	65.0	−70.0	70.0	−65.0	75.0
E (kcal/mol)	0	2.64	4.99	4.41	5.20	4.05	9.26	10.80	4.76	9.31

[a] Each model has a 2_1 helical conformation giving the measured fiber period of 6.7 Å. All energies are given relative to the 49.85 kcal/mol value of the g–tA model. A and B correspond to the backbone conformations ttg$^-$g$^-$ and ttgg, respectively.

Table 2. Comparison of Calculated and Observed Relative Intensities of the Electron Diffraction Patterns for Different Backbone and Side-Chain Conformations in the $P2_12_12_1$ Space Group[a]

*hk*0[a]	g–tA	g–tB	ttA	ttB	gtA	gtB	g–gA	g–gB	g–g–A	g–g–B
110 (vs)	vs	vs	vs	vs	vs	vs	vs	s	vs	vs
210 (vs)	vs	vs	vs	vs	vs	vs	vw	vw	vw	vs
200 (vs)	vs	vs	s	vs	vs	vs	vs	vs	s	vs
320 (w)	w	s	w	s	w	w	w	w	w	s
others (vw)	vw	s(020), m(220)	vw	m(120)	vs(020), m(310, 140)	vw	vw	vw	vs(020)	s(020, 040)

[a] The experimental intensities are given in the first column: vs = very strong, vw = very weak, s = strong, w = weak, and m = middle. These reflections, indicated in brackets, are easily visible from the simulated patterns but are ambiguous from the experimental observation.

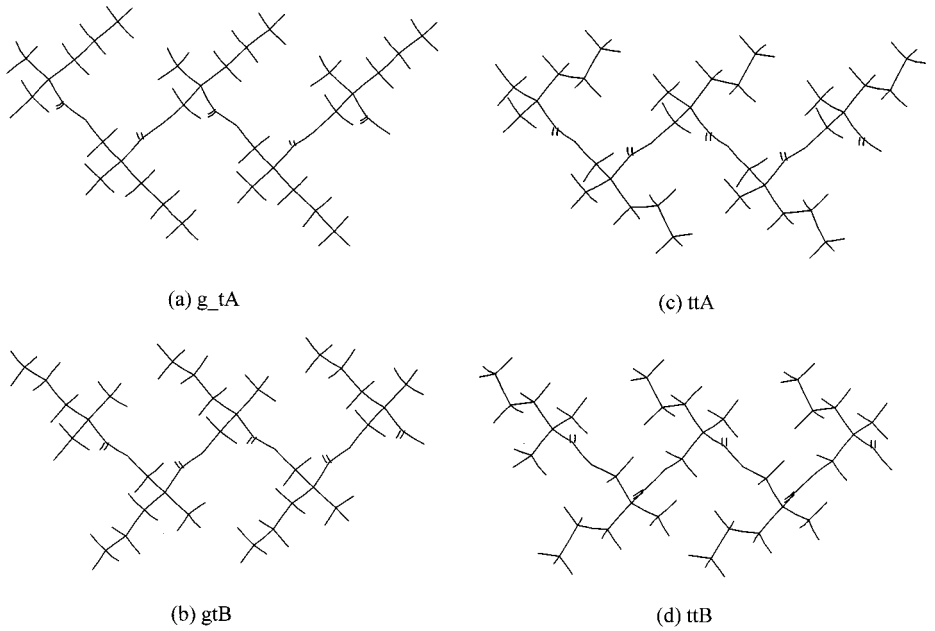

Figure 5. Four rigid packing models used for the flexible energy minimization: (a) g–tA, (b) gtB, (c) ttA, and (d) ttB.

and the g–tA or ttA side chain. Two chains are packed antiparallel in an orthorhombic lattice.

The electron diffraction patterns simulated for the *hk*0 reciprocal lattices are shown in Figure 6 for the g–tA and ttA models. The two simulated patterns show a good agreement with the experimental one: the 110, 200, 210, and 320 reflections are clearly observed. However, the ttA model shows an additional middle strong reflection that could be assigned as 120. The simulated patterns for the tilted sample, shown in Figure 7, also indicate that the g–tA model exhibits a better fit than the ttA model, with the latter having more intense 121 and 221 reflections than observed in the former.

In Figure 8, the experimental X-ray powder diffraction spectra[3] for the melt-crystallized (curve *a*) and the chloroform solution-cast (curve *b*) samples, after removal of the amorphous halo, are compared to those simulated for the flexible g–tA and ttA models (curves *c* and *d*, respectively); the *d* spacings and relative intensities of the stronger reflections are listed in Table 3. The previous crystal model[1] is also included in this table. The positions of the peaks observed were not calibrated with the *d* spacings of the electron diffraction data. Therefore, values obtained from the X-ray measurements are smaller than those obtained by electron diffraction, especially for low-layer reflections. However, because the same cell parameters *a* and *b* were used, both the simulated and experimental patterns exhibit similar *d* spacings for each diffraction peak. Some differences in intensity can easily be recognized, even between the two measured curves; at this moment, these differences remain unexplained.

As can be seen in Table 3, the g–tA, ttA, and the previous models show distinct differences in fiber periods with values of 6.31, 6.14, and 6.7 Å, respectively.

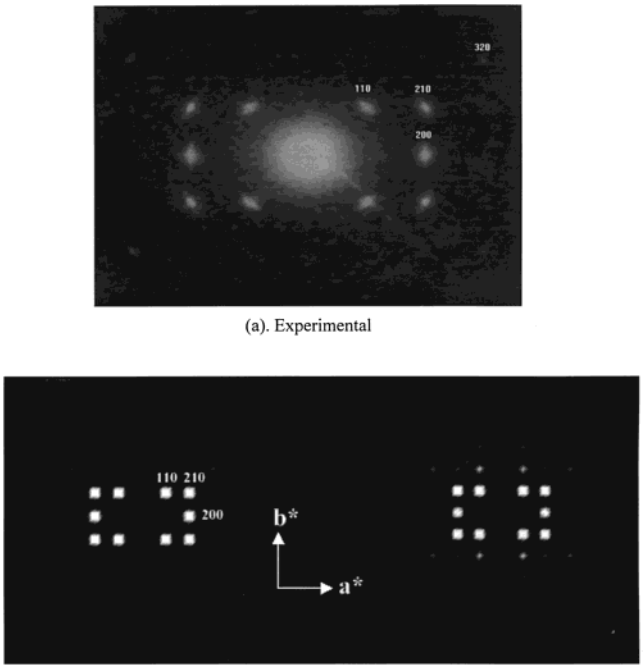

(a). Experimental

(b). g.tA (c). ttA

Figure 6. *hk*0 electron diffraction patterns (a* is vertical, b* is horizontal): (a) experimental pattern for a melt-crystallized sample, (b) calculated pattern for the g–tA model, and (c) calculated pattern for the ttA model.

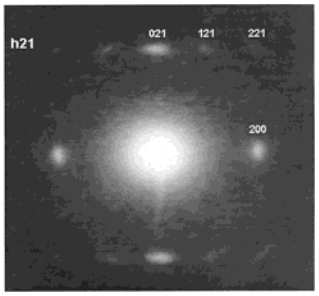

(a). Experimental

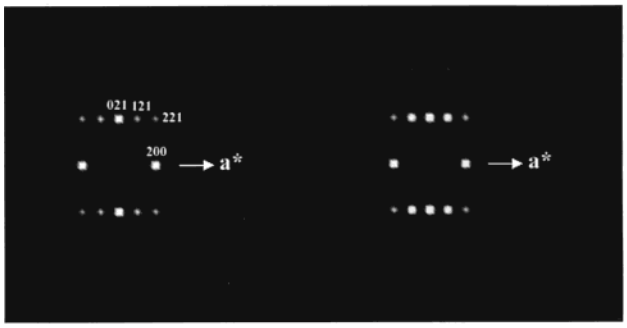

(b). g.tA (c). ttA

Figure 7. Electron diffraction patterns for the tilted sample: (a) experimental pattern for a melt-crystallized sample tilted by 40° about a*, (b) calculated 012 zone pattern for the g–tA model, and (c) for the ttA model.

For the flexible g–tA and ttA models, *c* was generated by a simultaneous intra- and intermolecular interaction optimization; for practical reasons, it was not constrained to the experimental value during the energy minimization. On the other hand, an analysis of the densities indicates that the fiber period of 6.7 Å is overestimated, and thus, the calculated cell density is underestimated (1.08 g/cm^3). The overestimation can easily be accounted for by the experimental error produced from the determination of *c* for the tilt sample. A decrease in *c* of only 3% could yield a calculated density larger than the measured value of 1.10 g/cm^3. Alternatively, the g–tA model gives a shorter fiber period and, then, a larger but acceptable density of 1.15 g/cm^3. The ttA model yields an even shorter fiber period and a density of 1.18 g/cm^3.

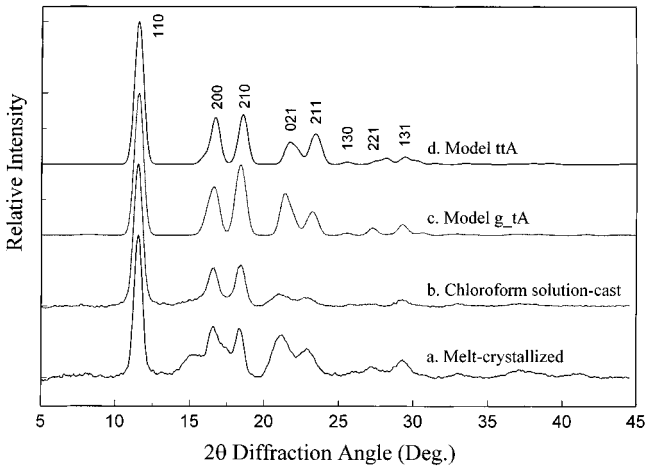

Figure 8. X-ray powder diffraction profiles of isotactic PMPPL: (a) experimental spectrum[2] after subtraction of the amorphous halo for a melt-crystallized sample, (b) experimental pattern for a chloroform solution-cast sample, (c) simulated spectrum for the g–tA model ($B = 20$ Å^2 for all atoms), and (d) simulated spectrum for the ttA model ($B = 10$ Å^2 for all atoms). The measured *d* spacings were calibrated by the electron diffraction data of a gold sample.

X-ray structure factors are also given in Table 3 for the separated peaks, for which thermal factors of 20 and 10 Å^2 were used for the g–tA and ttA models, respectively. These thermal factors were obtained from an optimization in the 0−30 Å^2 range in order to yield the lowest *R* factor. The structure factors for eight X-ray diffraction peaks also show an acceptable discrepancy factor *R* for both of the flexible g–tA and ttA models. By use of the reported X-ray structure factor data of Table 3, discrepancy factors of 0.20 and 0.17 were obtained for the g–tA and ttA models, respectively. If the melt-crystallized (curve *a* of Figure 8) data are used as reference, then values of 0.20 ($B = 15$ Å^2) and 0.20 ($B = 0$ Å^2) are obtained for the g–tA and ttA models, respectively. It is also interesting to note from Table 3 that the two models exhibit a similar statistical weight for the structure factor of each strong reflection; however, there is a meaningful exception: the ttA model shows a higher structure factor of the 101 reflection than that of the 200 reflection. Finally, the weaker 200 and 210 reflections and the much stronger 021 reflection of the flexible ttB model in the simulated X-ray profile further justifies its elimination.

In Table 4, the observed (F_o) and calculated (F_c) structure factors of the eight major *hk*0 and *h*21 diffraction spots observed in electron diffraction patterns are given for both of the flexible g–tA and ttA models. Both *hk*0 and tilted-specimen electron diffraction data were used in the calculation of the *R* factor. The use of *B* factors of 17 or 30 Å^2 leads to the lowest and most reasonable *R* factors, 0.17 for the g–tA model and 0.27 for the ttA model. By use of a smaller thermal

Table 3. Observed and Calculated *d* Spacings (d and d_c), Intensities (I_{rel}), and X-ray Powder Diffraction Structure Factors (F_o and F_c) for the Flexible g–tA and ttA Models[a]

indices	observed[3]			previous model[1]	g–tA				ttA			
							$F_c(B = 20$ Å$^2)$				$F_c(B = 10$ Å$^2)$	
hkl	d_o[b]	I_{rel}	m_i	d_c	d_c	F_o	individual	merged	d_c	F_o	individual	merged
110	7.49	100	4	7.67	7.67	4862	2431	4862	7.67	5813	2906	5813
020			2	5.55	5.55		308		5.55		721	
011			4	5.74	5.49		208		5.37		16	
	5.18	27				4320		4366		5166		4124
101			4	5.66	5.42		647		5.31		1810	
200			2	5.30	5.30		2917		5.30		1195	
120			4	4.92	4.92		1		4.92		154	
111			8	5.05	4.87		967		4.79		395	
	4.67	29				4559		5196		5452		5454
210			4	4.78	4.78		2208		4.78		2664	
021			4	4.28	4.17		2840		4.12		2174	
201			4	4.16	4.06		1306		4.01		1613	
	4.20	9				4536		6449		5424		6529
121			8	3.96	3.88		559		3.84		1289	
211	3.83	7	8	3.89	3.81	3639	787	2227	3.77	4351	1442	4080
130	3.43	2	4	3.49	3.49	995	259	519	3.49	1190	477	954
221			8	3.33	3.28		550		3.25		448	
	3.27	2				1516		1613		1813		4059
031			4	3.24	3.19		26		3.17		1802	
002			2	3.35	3.16		296		3.07		969	
131			8	3.10	3.06		799		3.04		1143	
	3.04	5				3293		2375		3937		3234
230			4	3.03	3.03		13		3.03		17	
012			4	3.21	3.04		365		2.96		2	
density (g/cm^3)	1.10	1.10	1.10	1.08	1.15	1.15	1.15	1.15	1.18	1.18	1.18	1.18
c (Å)				6.70	6.31	6.31	6.31	6.31	6.14	6.14	6.14	6.14

[a] The observed data are from the chloroform solution-cast sample. [b] These d spacings have not been calibrated by electron diffraction data of the gold-deposited samples.

Table 4. Observed (F_o) and Calculated (F_c) Electron Diffraction Structure Factors for the g–TA and TtA Models

				g–tA ($B = 17$ Å^2)		ttA($B = 30$ Å^2)	
sample	hkl	m_i	d_c (Å)	F_c	F_o	F_c	F_o
$hk0$ plane	1 1 0	4	7.67	236	444	211	352
	2 0 0	2	5.30	529	529	420	420
	2 1 0	4	4.78	411	390	309	310
	3 2 0	4	2.98	29	73	14	58
tilted	2 0 0	2	5.30	529	526	420	420
	0 2 1	4	4.17	532	532	366	425
	1 2 1	8	3.88	96	172	62	138
	2 2 1	8	3.28	94	91	51	73
R				0.17	0.17	0.27	0.27

factor B of 10 Å^2, the g–tA and ttA model leads to larger R factors of 0.19 and 0.30, respectively. It means that the g–tA model is more reasonable than that of the ttA model from the electron diffraction point of view.

Energetically, for an isolated single chain, an energy difference of 1.65 kcal/mol/RU (RU denotes the repeat unit) is found between the g–tA and ttA models. This large difference between single chains may result from artifacts because a constrained helical algorithm was used. After the flexible energy minimization of the crystal structure, both of the g–tA and ttA models have very close intramolecular energies (18.9 kcal/mol/RU for the g–tA and 18.5 kcal/mol/RU for the ttA models) and competitive packing energies (−36.5 and −37.1 kcal/mol/RU, respectively). It is seen in Table 5 that the intramolecular van der Waals interaction has balanced this energy difference between the two single chains. Intermolecularly, contributions from the Coulombic and van der Waals interactions are nearly balanced in the two models. On the other hand, both of the gtB and ttB models yield higher packing energies (−27.7 and −30.3 kcal/mol/RU, respectively) than those of the g–tA and ttA models; the gtB model also gives a relative intramolecular energy higher by about 10 kcal/mol/RU. By consideration of the simulation of the electron diffraction data, the gtB and ttB models can be reasonably eliminated.

It should be noted that the present g–tA and ttA models were derived from a combination of energy minimization and refinement against diffraction data, but the atoms and chain positions were never optimized with diffraction data. This optimization would undoubtedly lead to lower values of R. In fact, the use of relatively large B factors (above 10 Å^2) implies that the energy-minimized models contain some distortions from the real one. It is possible that the energy-minimized method combined with the constrained least-squares method[9,10] could give a better fit but without changing the final structure in a significant way. We will discuss this point in a later article.

The packing forms for the flexible g–tA and ttA models are given in Figure 9. Table 6 reports the fractional coordinates of one asymmetric unit of the two models. The shortest distance between two nonbonded atoms is 2.4 Å for the H···H pair. One can easily identify the same packing style in the two models. However, the g–tA model projected in the $hk0$ plane is more extended than that in the ttA model. Table 7 also indicates some structural differences between these two models with the backbone and side-chain dihedral angles of the rigid

Table 5. Interaction Energies[a] for the Four Flexible Models

	intramolecular				intermolecular			
model	$E_{repulsion}$	$E_{dispersion}$	$E_{Coulombic}$	E_{intra}	$E_{repulsion}$	$E_{dispersion}$	$E_{Coulombic}$	$E_{packing}$
g−tA	102.5	−95.2	11.6	18.9	20.5	−40.1	−16.9	−36.5
ttA	107.5	−100.6	11.6	18.5	23.1	−41.2	−19.0	−37.1
gtB	102.6	−94.1	20.6	29.1	19.3	−37.4	−9.6	−27.7
ttB	110.7	−105.2	11.7	17.2	24.4	−41.5	−13.2	−30.3

[a] Measured in kilocalorie per mole per repeat unit.

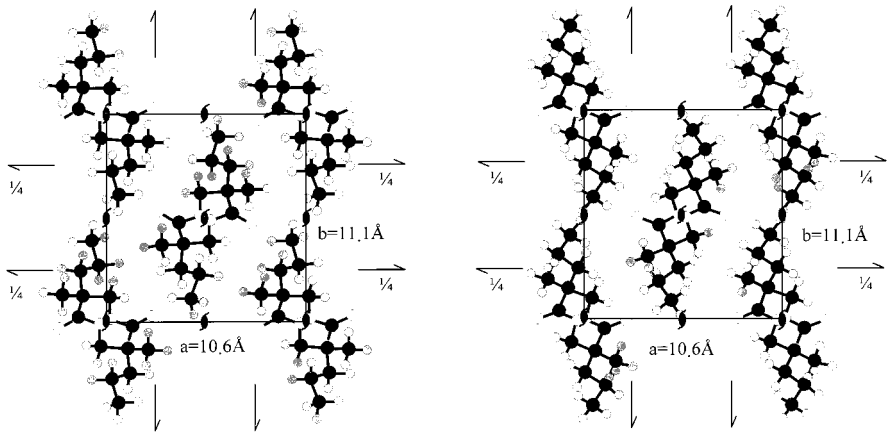

(a) ttA (b) g.tA

Figure 9. Projections of the orthorhombic unit cell along the *c* axis for (a) the g−tA model and (b) the ttA model.

Table 6. Fractional Coordinates of the Final g−tA and ttA Models Obtained with the Flexible Approach

	g−tA			ttA		
atom	*x*	*y*	*z*	*x*	*y*	*z*
C1	0.802 64	0.393 97	0.000 00	0.771 63	0.382 41	0.000 00
H1(C1)	0.834 24	0.321 27	−0.109 80	0.787 18	0.303 15	−0.105 03
H2(C1)	0.881 69	0.416 39	0.109 74	0.848 56	0.384 56	0.120 88
C2	0.684 82	0.349 77	0.130 07	0.639 06	0.372 20	0.107 02
C4	0.581 11	0.302 25	−0.025 03	0.533 84	0.368 07	−0.068 29
H1(C4)	0.495 09	0.276 23	0.064 04	0.440 02	0.359 15	0.006 60
H2(C4)	0.553 89	0.369 75	−0.148 05	0.532 70	0.448 62	−0.172 95
H3(C4)	0.615 80	0.221 80	−0.111 22	0.548 03	0.289 20	−0.174 25
C5	0.731 21	0.247 90	0.285 59	0.627 13	0.253 26	0.239 71
H1(C5)	0.808 02	0.282 64	0.390 24	0.636 84	0.178 52	0.121 45
H2(C5)	0.775 47	0.178 07	0.181 94	0.529 64	0.246 66	0.303 01
C6	0.633 12	0.185 21	0.430 81	0.718 55	0.227 10	0.427 70
H1(C6)	0.582 11	0.252 04	0.530 49	0.816 07	0.219 20	0.366 47
H2(C6)	0.561 45	0.140 00	0.329 12	0.718 35	0.301 38	0.546 48
C7	0.694 79	0.091 44	0.579 25	0.681 70	0.110 30	0.543 68
H1(C7)	0.624 59	0.044 58	0.680 59	0.742 16	0.092 32	0.685 21
H2(C7)	0.744 69	0.022 58	0.483 00	0.583 65	0.114 22	0.602 61
H3(C7)	0.764 18	0.133 41	0.689 12	0.689 41	0.032 64	0.433 29
C3	0.635 62	0.456 24	0.265 29	0.616 26	0.479 17	0.264 07
O2	0.529 46	0.494 41	0.267 83	0.517 44	0.529 40	0.295 18
O1	0.729 79	0.504 55	0.387 64	0.723 88	0.511 34	0.369 33

chains listed in brackets for comparison. After the flexible energy minimization, the backbone and side-chain torsion angles are somewhat distorted from the original 2_1 helices. The most significant deviations occur for the backbone torsion angles, especially for τ and ψ. However, ψ is much closer to 180° than it is to τ after the flexible energy minimization, which is in agreement with an early study of α-polypivalolactone.[12] Both models lead to a greater deviation (10∼20°) for ϕ.

Thus, it appears that the rigid procedure of energy minimization cannot directly give for PMPPL an acceptable fit with the experimental X-ray diffraction data because the initial conformation used is too different from the real one. However, it can indeed be used to exclude unreasonable conformations. For melt-crystallized PMEPL,[8] both rigid and flexible procedures led to reasonable results because the final conformation was very close to the starting planar zigzag conformation, which was obtained from energy minimization of a single chain. Variation to some extent in the fiber period of a 2_1 helical single chain of PMPPL could generate a series of low minima, and an investigation of the rigid-body packing[8] of these conformations could produce results similar to those obtained from the flexible procedure, but this approach would require a much longer period of time.

In addition to the 2_1 helical conformation described here, the polyesters based on the substituted poly(β-propiolactone) backbone also exhibit a planar zigzag conformation with a fiber repeat distance of 4.75 Å.[1,4,8] A change in conformation from a 2_1 helix to a fully extended chain, called the $\alpha-\beta$ phase transformation, can be realized by stretching or annealing. These phenomena have been reported for poly(pivalolactone),[12,23] PMEPL,[1,2] atactic PMPPL,[26] poly(α-phenyl-α-ethyl-β-propiolactone),[27] and polylactide.[5]

In this series of polyesters, the size of the side chain is an important factor controlling the formation of the crystalline phase. For poly(pivalolactone),[12,23] the α, β, and γ crystal forms have been observed and refined by energy calculations. For isotactic PMEPL,[28] the planar zigzag backbone conformation with a trans side chain has an energy difference of 0.74 kcal/mol/RU relative to the 2_1 helical backbone conformation with a g− side chain. For isotactic PMPPL, the energy difference increases to 0.94 kcal/mol/RU between a planar zigzag backbone conformation with a tt side chain and a 2_1 helical backbone conformation with a g−t side chain. It is then suggested that, when increasing the size of the side chain, it becomes more difficult to induce the β form. No experimental evidence of the presence of a γ form has been found so far for PMEPL and PMPPL.

Isotactic polylactide is a simpler optically active polylactone, with a $[CH(CH_3)\text{-}COO]_n$ motif, than poly-

Table 7. Geometrical Features of Simulated PMPPL Crystal Structures for the Flexible g⁻tA and ttA Models Packed in the $P2_12_12_1$ Space Group

	internal coordination	g⁻tA	ttA
bond lengths (Å)	C(1)−C(2)	1.561	1.555
	C(2)−C(3)	1.536	1.549
	C(3)−O(1)	1.360	1.359
	O(1)−C′(1)	1.420	1.422
	C(3)−O(2)	1.202	1.202
	C(2)−C(4)	1.547	1.551
	C(2)−C(5)	1.560	1.557
	C(5)−C(6)	1.536	1.535
	C(6)−C(7)	1.530	1.530
bond angles (deg)	C′(1)−(1)−C(3)	118.8	119.7
	O(1)−C(3)−C(2)	110.7	111.5
	O(2)−C(3)−C(2)	126.6	126.2
	O(1)−C(3)−O(2)	122.8	122.3
	C(1)−C(2)−C(3)	107.8	110.4
	C(1)−C(2)−C(4)	111.1	111.0
	C(1)−C(2)−C(5)	106.8	110.9
	C(3)−C(2)−C(4)	110.7	110.0
	C(3)−C(2)−C(5)	109.5	108.2
	C(4)−C(2)−C(5)	110.7	106.3
	C(2)−C(5)−C(6)	118.1	120.2
	O′(1)−C(1)−C(2)	111.0	109.0
	C(5)−C(6)−C(7)	111.4	110.4
torsion angles[a] (deg)	τ, C(2)−C(3)−O(1)−C′(1)	176.2 (−175.0)	172.2 (−175.0)
	ψ, C(3)−O(1)−C′(1)−C′(2)	178.9 (191.6)	178.0 (190.4)
	η, O″(1)−C(1)−C(2)−C(3)	−55.3 (−58.5)	−63.9 (−68.1)
	ϕ, C(1)−C(2)-C(3)−O(1)	−53.0 (−65.0)	−36.1 (−55.0)
	ω_a, C(4)−C(2)-C(5)−C(6)	−57.4 (−60.0)	179.6 (180.0)
	ω_b, C(2)−C(5)-C(6)−C(7)	−177.8 (−180.0)	175.6 (180.0)

[a] Values in brackets denote the torsion angles of the rigid models calculated from the helical algorithm.[11,12]

(pivalolactone), PMEPL and PMPPL; i.e., it contains two carbon atoms on its backbone per repeat unit instead of three. It has been found[5] that pure poly(L-lactide) is able to crystallize in an α-form with a 10_3 helical conformation or in a γ-form with a 3_1 helical conformation, which is a slightly extended conformation as compared to the 10_3 helix. Previous energy analyses[5,22] demonstrate that the 3_1 helix is less stable than the 10_3 helix for the homopolymer crystal. A careful examination of the polylactide geometry indicates that it cannot crystallize in a 2_1 helical conformation, because the ester groups[5,8,12,18,19] adopt a near-planar trans conformation (although there are some distortions) in all cases. In addition, a planar zigzag conformation has never been found for this polymer, which could be due to the intramolecular interactions rather than the intermolecular interactions because the third backbone torsion angle favors a gauche rather than a trans conformation according to the intramolecular interactions. In contrast, the planar zigzag conformation of isotactic and atactic PMEPL[1,8] and of atactic PMPPL[22] can be stabilized by intermolecular interactions, although the preference is given to the 2_1 helical conformation by the intramolecular interactions.

Conclusions

The crystal structure of isotactic PMPPL has been determined on the basis, on one hand, of conformational energy and packing energy calculations and, on the other hand, of X-ray and electron diffraction data. Two chains having a 2_1 helical backbone ttg^-g^- conformation (model A), with g⁻t or tt side chains, corresponding to the two lowest energy minima of the isolated chain, were packed antiparallel in the $P2_12_12_1$ space group. Investigations of the density, fiber period, packing energy, electron diffraction patterns, X-ray powder diffraction profiles, and structure factors yielded a satisfactory agreement with the experimental data. Both the g⁻tA and ttA models have led to the lowest energy packing and reasonable X-ray structural factors. However, the g⁻tA model shows a better agreement with the experimental cell density and electron diffraction pattern than does the ttA model, either visually or quantitatively. No significant difference was found between the total intra- and intermolecular energies of the two models.

Acknowledgment. The authors acknowledge the financial support of the National Sciences and Engineering Research Council of Canada and the Department of Education of the Province of Quebec (FCAR program). Z.H. also expresses his thanks to Drs. Josée Brisson and Anna M. Ritcey for useful discussions. We finally thank Dany Bussières (Département de biologie, Université Laval) for his help in image analysis.

References and Notes

(1) Ritcey, A. M.; Brisson, J.; Prud'homme, R. E. *Macromolecules* **1992**, *25*, 2705.
(2) Ritcey, A. M.; Prud'homme, R. E. *Macromolecules* **1992**, *25*, 972.
(3) Ritcey, A. M.; Prud'homme, R. E. *Macromolecules* **1993**, *26*, 1376.
(4) Soldera, A.; Prud'homme, R. E. *Macromolecules* **1997**, *30*, 3107.
(5) Okihara, T.; Tsuji, M.; Kawagichi, A.; Katayama, K. *J. Macromol. Sci., Phys.* **1991**, *B30*, 119.
(6) Brizzolara, D,; Cantow, H.-J.; Diederichs, K.; Keller, E.; Domb, A. J. *Macromolecules* **1996**, *29*, 191.
(7) Brochu, S.; Prud'homme, R. E.; Barakat, I.; Jérôme, R. *Macromolecules* **1995**, *28*, 5230.
(8) He, Z.; Brisson, J.; Prud'homme, R. E.*Macromolecules* **1998**, *31*, 8218.
(9) Arnott, S.; Wonacott, A. J. *Polymer* **1963**, *7*, 157.
(10) Tadokoro, H. *Structure of Crystalline Polymers*; Robert E. Krieger Pub. Corp.: Malabar, Florida, 1990.

(11) Tripathy, S. K.; Hopfinger, A. J.; Taylor, P. L. *J. Phys. Chem.* **1981**, *85*, 1371.
(12) Ferro, R.; Bruckner, S.; Meille, S. V.; Ragazzi, M. *Macromolecules* **1990**, *23*, 1676.
(13) Sorensen, R. A.; Liau, W. B.; Boyd, R. H. *Macromolecules* **1988**, *21*, 194.
(14) Rutledge, G. C.; Suter, U. W. *Macromolecules* **1991**, *24*, 1921.
(15) Ferro, D. R.; Meille, S. V.; Bruckner, S. *Macromolecules* **1998**, *31*, 6926.
(16) Shimanouchi, T.; Mizushima, S. *J. Chem. Phys.* **1955**, *23*, 707.
(17) Miyazawa, T. *J. Polym. Sci.* **1961**, *55*, 215.
(18) Flory, P. J. *Statistical Mechanics of Chain Molecules*; Interscience: New York, 1969.
(19) Mattice, W. L.; Suter, U. W. *Conformational Theory of Large Molecules. The Rotational Isomeric State Model in Macromolecular Systems*; Wiley: New York, 1994.
(20) Manus for the simulation software: Insight II 4.0.0, Discover 4.0.0 and Polymer 4.0.0, Biosym/MSI **1997**.
(21) Iribarren, I.; Aleman, C.; Bou, J. J.; Munoz-Guerra, S. *Macromolecules* **1996**, 29, 4397.
(22) Cornibert, J.; Marchessault, R. H. *Macromolecules* **1975**, *8*, 296.
(23) Prud'homme, R. E.; Marchessault, R. H. *Macromolecules* **1974**, *7*, 541.
(24) Dorset, D. L. *J. Electron Microsc. Tech.* **1985**, *2*, 89.
(25) Henry, N. F. M.; Lonsdale, K. *International Tables for X-ray Crystallography*, Vol. 1, Symmetry Groups; Kynoch Press: Birmingham, 1952.
(26) Cornibert, J.; Marchessault, R. H.; Allegrezza, E. A., Jr.; Lenz, R. W. *Macromolecules* **1973**, *6*, 676.
(27) Lenz, R. W.; d'Hondt, G.; Bigdeli, E. *Polym. Prepr.* **1977**, *18*, 81.
(28) Unpublished results.

MA981549+